



### **Science Arts & Métiers (SAM)**

is an open access repository that collects the work of Arts et Métiers Institute of Technology researchers and makes it freely available over the web where possible.

This is an author-deposited version published in: <https://sam.ensam.eu>  
Handle ID: <http://hdl.handle.net/10985/9567>

#### **To cite this version :**

Michal GZYL, Andrzej ROSOCHOWSKI, Sonia BOCZKAL, Lech OLEJNIK, Raphaël PESCI - In situ analysis of the influence of twinning on the strain hardening rate and fracture mechanism in AZ31B magnesium alloy - Journal of Materials Science - Vol. 50, n°6, p.2532-2543 - 2015

Any correspondence concerning this service should be sent to the repository

Administrator : [scienceouverte@ensam.eu](mailto:scienceouverte@ensam.eu)



# In situ analysis of the influence of twinning on the strain hardening rate and fracture mechanism in AZ31B magnesium alloy

Michał Gzyl · Raphaël Pesci · Andrzej Rosochowski ·  
Sonia Boczek · Lech Olejnik

**Abstract** The influence of twinning on the strain hardening rate and fracture mechanism in AZ31B magnesium alloy was studied in this work by in situ microstructural analysis during tensile testing in a chamber of scanning electron microscope. Three types of samples used in this study were obtained by (1) extrusion (as-supplied), (2) I-ECAP and (3) I-ECAP followed by side upsetting. Microstructures, textures and mechanical properties were examined after each processing step. An analytical equation was used to describe flow stress curves of the samples which exhibited various modes of deformation (1) only by slip, (2) dominated by tensile twinning followed by slip and (3) dominated by contraction twinning followed by slip. It was shown that tensile twinning increases strain hardening rate, while the opposite is observed for contraction

twinning. The effective Schmid factors for slip in volumes deformed by tensile and contraction twinning were determined in this work using modelling approach as 0.215 and 0.45, respectively. Contraction twinning was also revealed to be responsible for an earlier fracture of the extruded sample subjected to tension, since microcracking was shown explicitly to be initiated within twins.

## Introduction

Magnesium alloys are very promising materials for various industries, e.g. automotive and aerospace, due to their low density. However, the hexagonal close-packed (hcp) crystallographic structure of magnesium has a strong influence on its formability and mechanisms of plastic deformation are very complex. Twinning in magnesium alloys is observed very often as this deformation mode is required to accommodate plastic strain due to an insufficient number of slip systems available at room temperature. Slip on the basal plane is impossible if the  $c$ -axis of the hexagonal cell is aligned parallel to the direction of tension/compression. In this case, twinning or non-basal slip need to be activated to enable plastic deformation. Generally, the former operates at room temperature, while the latter dominates above 200 °C [1].

Two main modes of twinning are distinguished in the literature [1–3]: (1)  $\{10\text{--}12\}$  ‘tensile twinning’, which enables extension along the  $c$ -axis, and (2)  $\{10\text{--}11\}$  ‘contraction twinning’, which enables compression along the  $c$ -axis. The secondary contraction twinning of the volume already deformed by the tensile twin was also revealed and it was recognised in the literature as  $\{10\text{--}12\}$ – $\{10\text{--}11\}$  ‘double twinning’ [2, 3], which can be responsible for an earlier material fracture due to strain localisation in the

twinning regions [1]. More recent studies showed that twin-sized voids were revealed in the regions previously occupied by double twins in samples subjected to plane strain compression [4] and tension [5]. Moreover, plate-like voids were observed on the fracture surface of AZ31 subjected to tension, which was attributed to the operation of a twinning-related mechanism of voids formation [6].

The activation of various deformation mechanisms, including {10–12} tensile twinning and slip on basal and non-basal planes in rolled magnesium samples of AZ31, was investigated through experiments and modelling using a semianalytical Sachs model developed by Barnett et al. [7]. Later, they used this model to investigate the influence of tensile twinning on the strain hardening rate and uniform elongation in extruded samples [8]. It was shown that tensile twinning can be responsible for an increased uniform elongation in testing perpendicular to the extrusion direction (ED). Modelling results have also confirmed previous observations that tensile twinning can increase flow stress due to interactions between moving dislocations and twin boundaries in hcp metals [9, 10]. On the other hand, it was suggested in [5] that contraction mode of twinning can lead to fracture during tensile testing along ED. However, the phenomenological model developed in that work to describe the effect of contraction twinning on the flow behaviour has not been used to quantitatively compare the results obtained from testing parallel and perpendicular to ED.

The aim of the current work was to use the model proposed in [7] to describe flow stress curves reflecting various modes of deformation (1) only by slip, (2) dominated by tensile twinning followed by slip and (3) dominated by contraction twinning followed by slip. A novel continuous process of severe plastic deformation (SPD), called incremental equal channel angular pressing (I-ECAP) [11, 12], was used in this work to produce fine-grained billets from AZ31B magnesium alloy [13]. Additionally, bars processed by four passes of I-ECAP were subjected to side upsetting. Finally, tensile testing and microstructural characterisation were conducted for three types of flat samples (1) extruded (as-supplied), (2) I-ECAPed and (3) I-ECAPed followed by side upsetting. The in situ and ex situ tensile tests were performed to investigate effects of twinning on the strain hardening rate and fracture in the billets obtained by different deformation paths.

## Materials and methods

The material used in the present work was AZ31B (as-fabricated) wrought magnesium alloy with the chemical composition given in Table 1. It was purchased in the form

of hot-extruded rods with the diameter of 16 mm from Magnesium Elektron (Manchester, UK). Square cross-section bars, with the dimensions  $10 \times 10 \times 120 \text{ mm}^3$ , were machined from the rods along ED and subjected to I-ECAP. The double-billet variant of I-ECAP [14], with a  $90^\circ$  angle between channels, was realised on a 1 MN hydraulic servo press. Four passes with a billet rotation by  $90^\circ$  after each pass, known in the literature as route  $B_C$  [15], were conducted at  $250 \pm 2^\circ\text{C}$ . Plastic strain was introduced using a punch which followed a sine wave signal defined by peak-to-peak amplitude  $A = 2 \text{ mm}$  and frequency  $f = 0.5 \text{ Hz}$ . Material feeding was realised by a motor-driven screw jack, synchronized with the reciprocating movement of the punch. Feeding stroke in each cycle was  $d = 0.2 \text{ mm}$ . After I-ECAP, the billet was rotated by  $90^\circ$  around its longitudinal axis (put on side) and upset from the initial thickness of 10 mm to 2 mm (equivalent to logarithmic strain of 1.6) using a hydraulic press with the capacity of 2.5 MN. Upsetting was conducted at  $200 \pm 5^\circ\text{C}$  using preheated and lubricated platens with the constant ram velocity  $0.1 \text{ mm s}^{-1}$ . The billets after four passes of I-ECAP and subsequent upsetting are shown in Fig. 1. The origin of the billet distortion after I-ECAP by route  $B_C$  was already discussed as related to strain rate sensitivity of non-uniformly strained material [16, 17]. The irregular shape of the I-ECAPed billet has influenced the sample appearance after upsetting.

Flat tensile specimens with the thickness of 2 mm and the strain gauge dimensions of  $4 \times 15 \text{ mm}^2$  were cut out along ED from the extruded, I-ECAPed, and upset samples. In situ tests of the extruded and upset specimens were performed using a screw-driven tensile stage placed inside a chamber of Jeol 7001FLV scanning electron microscope (SEM). Pulling was conducted at room temperature with the constant velocity of  $0.5 \text{ mm s}^{-1}$ , equivalent to the initial strain rate of  $3.3 \times 10^{-2} \text{ s}^{-1}$ . Cross-head displacement was measured using a LVDT displacement transducer. SEM images of the coarse-grained samples were taken at true strains: 0.008, 0.02, 0.03, 0.06, 0.08 and 0.087 (fracture strain). In the case of fine-grained samples, pulling was stopped to take pictures at true strains: 0.02, 0.03, 0.06, 0.13 and 0.19 (fracture strain). Additionally, ex situ microstructural characterisation was performed using optical and scanning electron microscopes for the I-ECAPed samples tested to true strains: 0.08, 0.15, 0.23 (fracture strain).

The extruded and upset samples were ground, polished and etched before putting into the SEM chamber; the I-ECAPed samples followed the same procedure after tensile testing. The preparation procedure included grinding using SiC paper P600 and P1200, mechanical polishing using polycrystalline suspensions with particle sizes: 9, 3 and  $1 \mu\text{m}$ , chemical treatment with nital and final polishing

**Table 1** Chemical composition limits (in weight percentile) of the AZ31B alloy used in this work (according to the supplied certificate of conformance)

	Al	Zn	Mn	Ca	Cu	Fe	Ni	Si	Mg
Maximum	2.5	0.7	0.2	–	–	–	–	–	–
Minimum	3.5	1.3	1.0	0.04	0.05	0.005	0.005	0.05	Balance

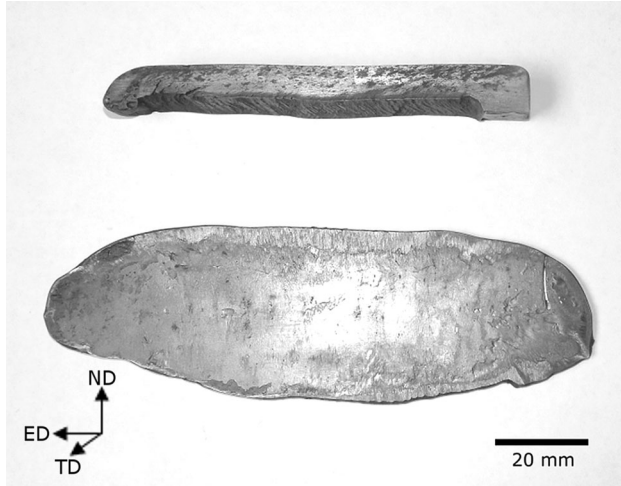


**Fig. 1** Samples after four passes of I-ECAP using route B<sub>C</sub> (*upper*) followed by side upsetting (*lower*); ED extrusion direction, ND normal direction, TD transverse direction

with 0.02  $\mu\text{m}$  alumina suspension. Then, the specimens were etched using acetic picral to reveal grain boundaries. The mean grain size was measured by the linear intercept method using Olympus analysis software. The ImageJ freeware software was used to evaluate the volume fraction of twinned grains. The dimensions of the examined zone were  $380 \times 280 \mu\text{m}^2$  and the magnification ratio was 330. EBSD maps were obtained after each step of processing using HRSEM FEI Inspect F50; the specimens were polished using ion milling technique on Leica RES101 machine. Step size for analysis was 0.3  $\mu\text{m}$  for the I-ECAPed and upset samples and 0.7  $\mu\text{m}$  for the extruded specimen. Microtextures were calculated from the obtained EBSD maps.

## Results

### Microstructures, textures and mechanical properties

The microstructure of the as-supplied rod was very heterogeneous with the average grain size of  $\sim 50$  and  $\sim 10 \mu\text{m}$  for coarse- and fine-grained zones, respectively (Fig. 2a). The occurrence of small grain colonies was attributed to

dynamic recrystallization during hot extrusion. Twins were not observed in the initial microstructure. It is apparent from Fig. 2d that the  $c$ -axes of the hexagonal cells are aligned perpendicular to ED; therefore, twinning is suspected to be operating in this specimen to accommodate compression along  $c$ -axis, which is confirmed later in this article by microstructural observations.

Processing by I-ECAP led to remarkable grain refinement ( $\sim 5 \mu\text{m}$ ) and microstructure homogenisation (Fig. 2b). Texture was also significantly changed as basal planes are now tilted at  $\sim 35^\circ$  to ED (Fig. 2e). Further upsetting at 200  $^\circ\text{C}$  slightly refined the grain size to  $\sim 4 \mu\text{m}$  (Fig. 2c). However, it is pronounced from the pole figure shown in Fig. 2f that basal planes are aligned almost parallel to ED of the obtained sheet; such fibre texture is usually observed after rolling of AZ31.

Mechanical properties of the extruded rod were significantly changed after I-ECAP by route B<sub>C</sub> (Fig. 3). The yield strength was lowered from 220 to 80 MPa with the simultaneous ductility enhancement from 0.09 to 0.23 of tensile true strain. A texture-related weakening of the I-ECAPed bars has been already thoroughly investigated in [13]. It was established that inclination of the  $c$ -axis of the hexagonal cell by  $\sim 35^\circ$  to tensile direction favoured slip on basal plane, which lowered yield stress. The similar texture was obtained in the current study.

The yield stress was increased from 80 to 145 MPa after upsetting of the I-ECAPed billet. Since the average grain size before and after upsetting is considered as negligible, the strength increase was attributed to the modification of texture. Basal planes are aligned at  $\sim 35^\circ$  to tensile direction during testing of I-ECAPed sample, which theoretically enables slip on basal plane with the lowest resolved shear stress (RSS). It is estimated from the pole figure displayed in Fig. 2f that  $c$ -axes are tilted at  $10\text{--}15^\circ$  to the tensile direction after upsetting, which increases RSS on basal plane and, as a consequence, rises yield stress of the material.

Strain hardening exponents,  $n$ , for AZ31B subjected to the different stages of processing are displayed in Fig. 3. The extruded rod exhibited a distinctive hardening behaviour which could be divided into two phases: (I) relatively intensive hardening ( $n_{\text{I}} = 0.14$ ) up to true strain  $\sim 0.025$  and (II) lower hardening rate ( $n_{\text{II}} = 0.08$ ) above  $\sim 0.025$ .



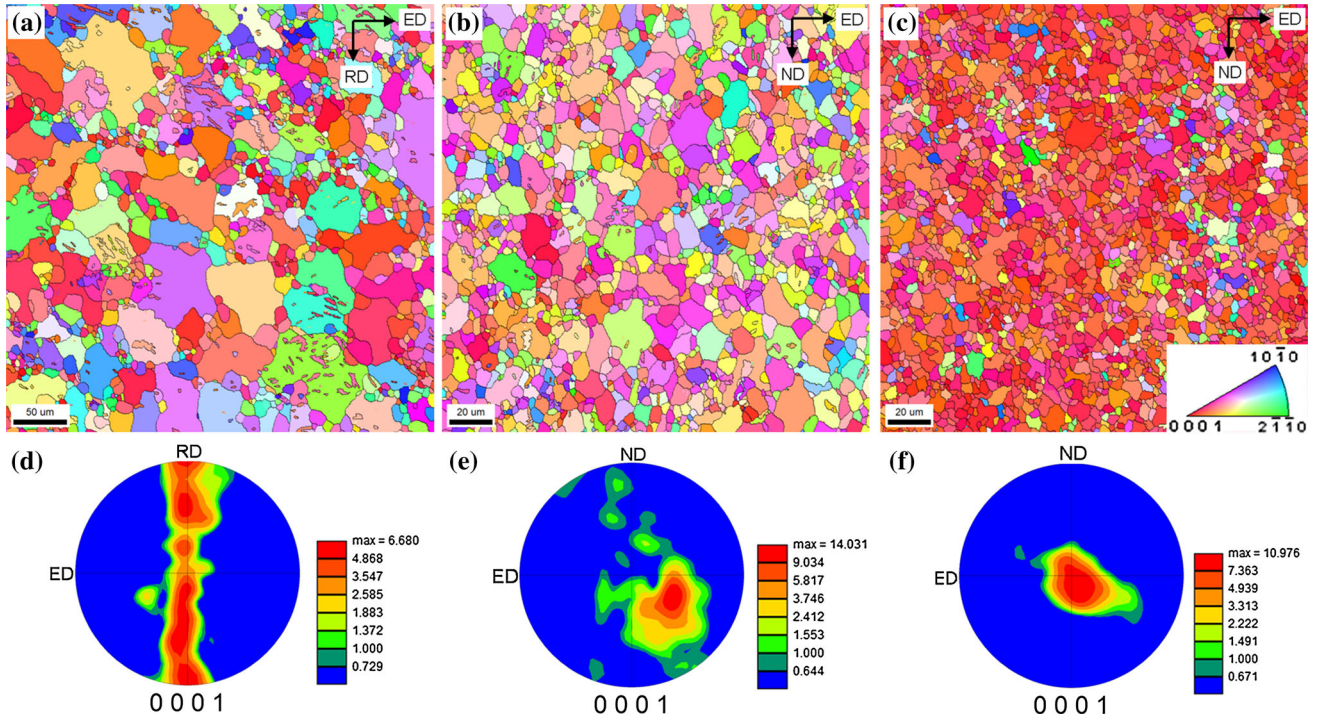


**Fig. 2** EBSD maps after (a) direct extrusion (as-supplied), (b) I-ECAP at 250 °C and (c) I-ECAP followed by upsetting at 200 °C; corresponding (0001) pole figures are shown in (d–f); *ED* extrusion direction, *RD* radial direction, *ND* normal direction, *TD* transverse direction

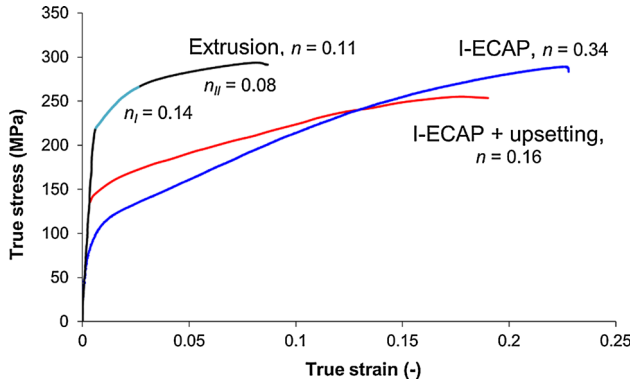


**Fig. 3** Mechanical properties of the AZ31B magnesium alloy samples after different stages of processing. Strain hardening exponents,  $n$ , are displayed for each sample. Two hardening stages with exponents  $n_I$  and  $n_{II}$  are distinguished for the extruded sample

The average strain hardening rate for this material was 0.11. The biggest slope ( $n = 0.34$ ) of the flow stress curve was obtained after I-ECAP at 250 °C. However, subsequent side upsetting decreased hardening exponent to  $n = 0.16$ . The different hardening rates of the examined samples are intriguing as they cannot be simply explained by the grain size effect. The microstructure evolution in the coarse- and fine-grained samples was studied in situ and ex situ and it will be presented in the following sections of this article in order to find a relation between the strain

hardening rate and deformation mechanisms occurring in the tested samples.

#### Microstructure evolution and fracture mechanism in extruded specimen

Figure 4a and b show microstructures of the extruded rod at strains 0.02 and 0.03, respectively. The occurrence of waving highlighted surface steps (Fig. 4a) was attributed to plastic deformation by dislocation movement. Density of the white waving lines was increasing with strain and the lines were becoming lighter which indicated that relief on the sample surface was rising. First twins, approximately 70  $\mu\text{m}$  long, were revealed in coarse grains in zones marked 1 and 2 at strain 0.03. Moreover, one of the observed twins appeared in the grain with a large amount of slip traces (detail 1 in Fig. 4a, b), which indicated that the initial orientation of the grain allowed for only limited amount of slip and further deformation must have been accommodated by twinning.

It is apparent that number of twins rose significantly with strain increasing from 0.03 to 0.087. Apart from the occurrence of new twins, the ‘old ones’ were continuously growing, as observed for twin 2 in Fig. 4b, which is also identified in Fig. 5a–c. The width of this twin rose from  $\sim 2$  to  $\sim 8$   $\mu\text{m}$  with strain increasing from 0.03 to 0.06 and continued to grow with strain, as shown in Fig. 5b and c.

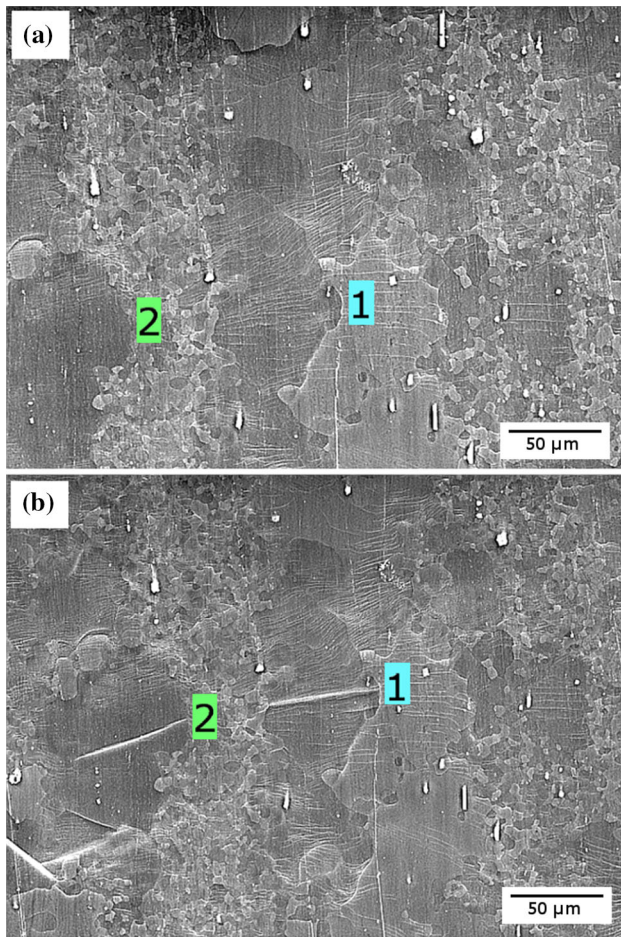


**Fig. 4** Microstructure evolution in the coarse-grained sample at true strains: 0.02 (a) and 0.03 (b). Tensile direction is vertical

Moreover, new twins appeared in grain 2 at strain 0.08 and they were also growing (Fig. 5c), almost completely consuming the grain at the last stage of deformation.

The nucleation of twins and their subsequent growth was not the only microstructural feature observed during this test. Twin 3 in Fig. 5a–c was growing with strain increasing from 0.06 to 0.08. However, its growth was stopped and a 14  $\mu\text{m}$  wide microcrack appeared in its place at strain 0.087, as seen in Fig. 5c. Other deformation zones were examined to clarify if the observed phenomenon was the common mechanism or only incidental one. As it is shown in Fig. 5d, more twin-sized cracks (marked as details 4) were revealed and their number was noticeably larger near the fracture zone. At the same time, formation of voids was not observed at any other sites than twins.

#### Microstructure and fracture mechanism in I-ECAPed specimen

Shear bands aligned parallel to the shear plane of I-ECAP were revealed in the I-ECAPed sample after tensile test

(Fig. 6a). It should be noted that they appeared during tensile testing and localisation of strain was not observed in the microstructure immediately after I-ECAP. Spacing between the bands was decreasing with pulling and it was also shown that most of the grains lying within bands were deformed by twinning (Fig. 6b). Therefore, the number of twinned grains rises along with increase of strain. The origin of shear bands formation is not explained in this study but the role of twinning is emphasised.

The fracture behaviour after I-ECAP was different from the extruded rod. It is apparent from Fig. 7 that the examined sample broke along the shear plane, which was also reported for the billets processed by routes A and C of I-ECAP [13]. Microstructural features such as twin-sized voids or intergranular fracture were not revealed in this case. However, the effect of microstructure on the fracture behaviour can be seen at the macroscopic level. The I-ECAPed sample is characterised by an even fracture surface inclined at  $\sim 45^\circ$  to the tensile direction, while extruded specimen showed a rugged fracture surface with dimples (Fig. 7). The former could be attributed to shear banding and the latter to twinning-related mechanism of failure (Fig. 5).

#### Microstructure evolution and fracture mechanism in I-ECAPed and upset specimen

Microstructure evolution of the fine-grained material from its initial state after I-ECAP followed by upsetting to tensile strain of 0.13 is shown in Fig. 8a–b. It is apparent that grains are elongated, e.g. grain 1 is stretched along the tensile axis from 11.7 to 13  $\mu\text{m}$  ( $\sim 11\%$ ). At the same time, some small grains ( $\sim 1\text{--}2\ \mu\text{m}$ ) were shown to be virtually not deformed; therefore, a different mechanism must have been activated to ensure stress compatibility on grain boundaries, e.g. grain boundary sliding (GBS). This conclusion is also supported by highlighted grain boundaries (Fig. 8b) and the literature results presented in [18], where GBS was shown to operate at room temperature in the fine-grained AZ31. In contrast to the extruded rod, twins have not been revealed at any stage of deformation in the upset specimen.

The fracture mechanism observed in the fine-grained samples produced by I-ECAP and upsetting was completely different from that in the coarse-grained ones. First microcracks were revealed on grain boundaries at strain 0.13, as shown between grains 1 and 2 in Fig. 8b. The growth and coalescence of the generated voids was much slower than in the case of coarse-grained material, as it enabled further deformation to 0.19 of true strain. Large voids observed near fracture zone are shown in Fig. 8c. Although the earlier stages of test indicated that the only failure mechanism is intergranular fracture, the images



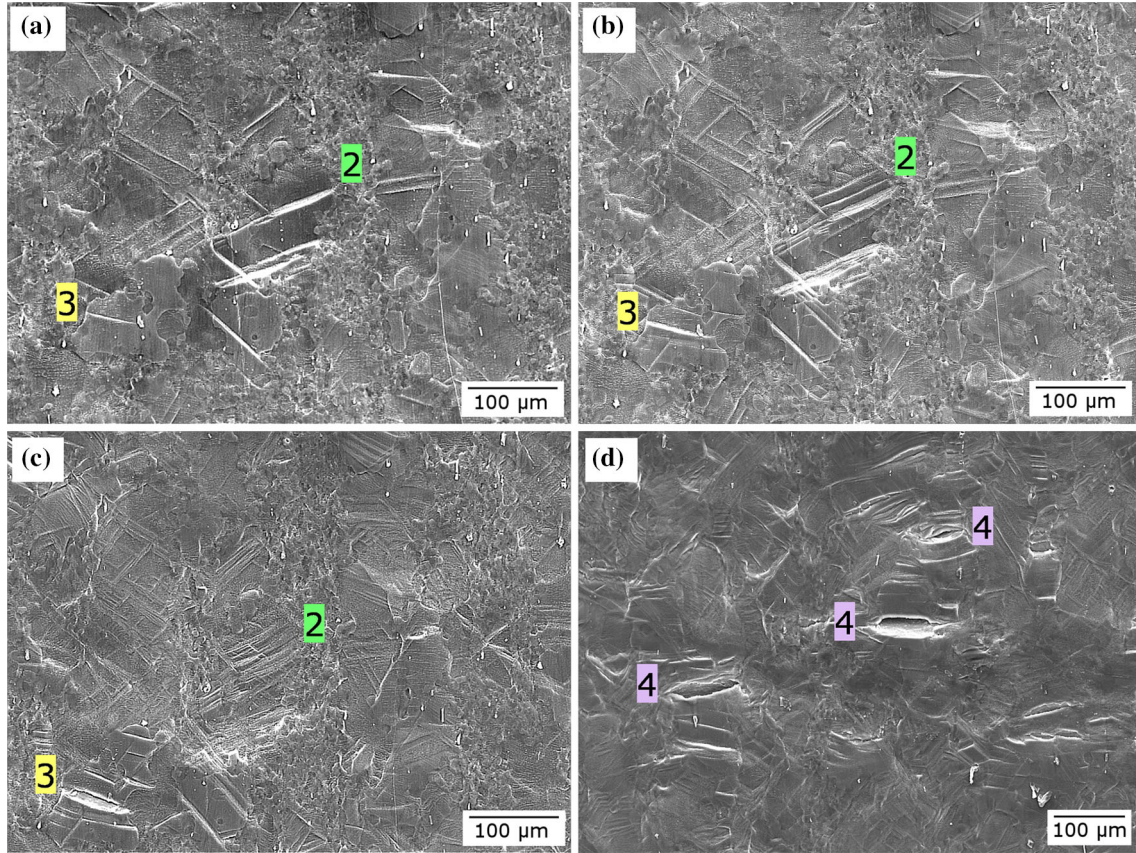


**Fig. 5** SEM images of the same area in the coarse-grained material at true strain: 0.06 (a), 0.08 (b), 0.087 (c). Twin-sized voids are revealed  $n$  (d). Tensile direction is vertical

taken in the deformation zone revealed that the mechanical shearing of grains has also contributed to the material damage (Fig. 8d).

## Modelling of the flow stress

### Model overview

The modelling part of this work was focused on investigating effects of the twinning activation on the flow behaviour of the extruded rod and I-ECAPed sample in tension. Attempts were made to describe the flow stress curves for all three samples using the semianalytical Sachs model developed by Barnett et al. [7], which allowed comparing the results obtained from this study with experimental and theoretical results derived from the literature [5, 7, 8].

The model was originally used to investigate the operation of twinning and basal slip in a rolled plate [7] and in an extruded rod [8] of AZ31 magnesium alloy. The ex situ observations performed using optical microscopy showed that twins were not present in the rolled plate pulled along

rolling and transverse directions [7]. Different behaviour was observed in the extruded rod, where  $\{10\text{--}12\}$  tensile twins were shown to be responsible for the increased strain hardening rate and enhanced uniform elongation in tension conducted perpendicular to ED [8]. The goal of the current work was to incorporate the effect of contraction twinning on the strain hardening rate and quantitatively compare the results with tensile twinning.

The general concept of the model is to divide the material volume into regions dominated by twinning ( $V_t$ ) and slip-dominated deformation ( $V_s = 1 - V_t$ ). Twinning and slip contributions to the flow stress are calculated separately in the particular zones and summed up in the final stage of calculations, according to the law of mixtures. The slip-dominated volume is a region where twinning is not operating and different mechanisms can be active in this zone, e.g. basal and non-basal slips. They are all treated in this model as only one deformation mode to simplify calculations. The volume fraction of twinned grains,  $V_t$ , is obtained experimentally from in situ and ex situ analysis conducted in the previous section.

Stresses in the different volumes are dependent on the effective Schmid factors for twinning ( $m_t$ ), slip in a



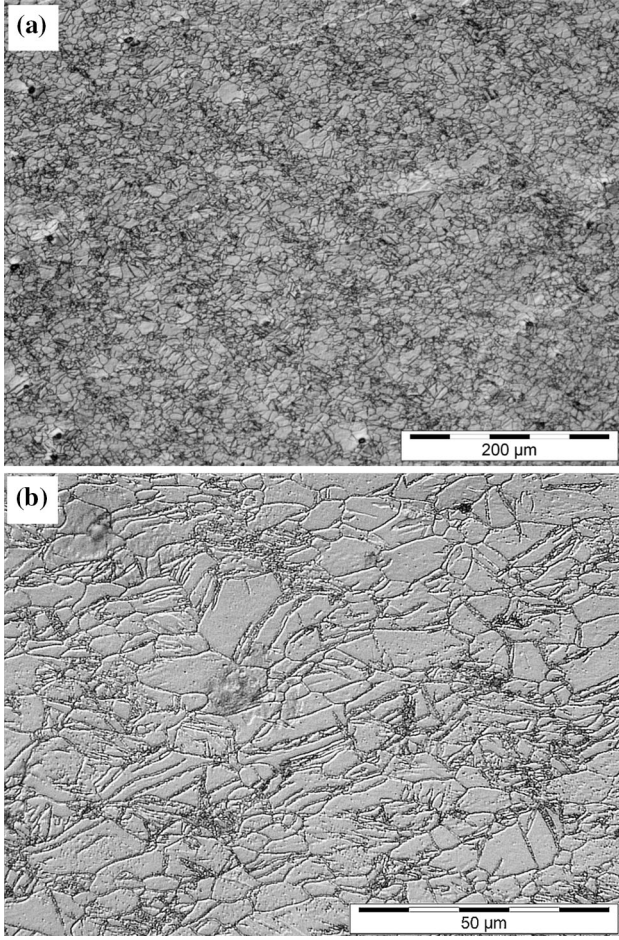


**Fig. 6** Microstructures of the I-ECAPed sample after tensile testing to fracture: (a) shear bands close to the fracture zone and (b) twinned and deformed grains within the shear band. Tensile direction is horizontal

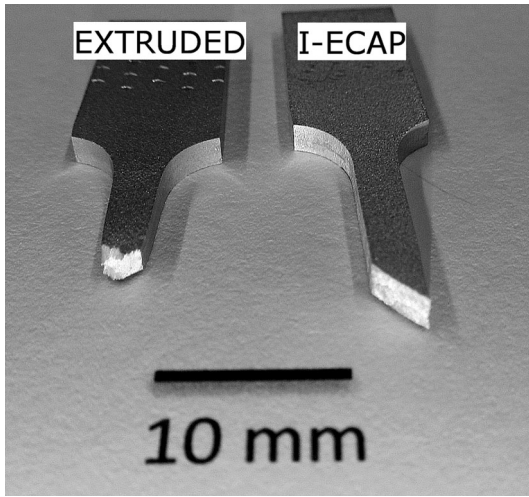


**Fig. 7** Fracture of the extruded rod and I-ECAPed bar subjected to tension

twinned volume ( $m_{II}$ ) and slip in a non-twinned volume ( $m_{III}$ ). The same as in the original model [7], parameters  $m_I$ – $m_{III}$  are fitting coefficients changing within range 0–0.5, according to the Schmid law. A higher Schmid factor indicates that deformation is easier to occur (stress level is lower) than in the case of a low Schmid factor.

It is assumed that three stresses contribute to the overall macroscopic stress:  $\sigma_I$ —twinning stress,  $\sigma_{II}$ —stress arising from a slip deformation in already twinned region,  $\sigma_{III}$ —stress in a region deformed only by slip. The partial stresses are multiplied by the volumes they operate in and summed up to give the overall macroscopic stress:

$$\sigma = dV_t \sigma_I + V_t \sigma_{II} + (1 - V_t) \sigma_{III} \\ = dV_t \frac{\tau_{0t}}{m_I} + V_t \frac{k}{m_{II}^{\eta+1}} \zeta + (1 - V_t) \frac{k}{m_{III}^{\eta+1}} \varepsilon^\eta, \quad (1)$$

where  $m_I$  is the effective Schmid factor for twinning and  $\tau_{0t}$  is the critical resolved shear stress (CRSS) for twinning,  $k$  is the magnitude of CRSS for all slip deformation modes not related to twinning,  $dV_t$  is the increment of the volume fraction of twinned grains,  $m_{II}$  is the effective Schmid factor for slip in twinned regions,  $\zeta$  is the arbitrary hardening coefficient of twinned volume and  $\eta$  is the hardening rate exponent (note that it is different from the hardening rate exponent  $n$  introduced in the experimental section of this work),  $V_t$  is the volume fraction of twinned grains,  $m_{III}$  is the effective Schmid factor for slip in non-twinned regions,  $\varepsilon$  is macroscopic strain.

#### Evaluation of the volume fraction of twinned grains

The observations performed using optical (OM) and scanning electron microscopy (SEM) enabled evaluating the volume fraction of twinned grains in the examined zones. Five experimental points from the in situ analysis in SEM and three points from the ex situ observations using OM were obtained for the extruded and for the I-ECAPed samples, respectively. It is apparent from Fig. 9 that twinning rates in the coarse- and fine-grained samples were different. Coarse grains underwent twinning more rapidly, while the I-ECAP specimen exhibited much lower rate of twinning. This observation is in good agreement with the experimental results obtained by Koike et al. [19], where increase in twin area fraction in the rolled plate with the average grain size of 86  $\mu\text{m}$  was much lower than in the fine-grained (17  $\mu\text{m}$ ) AZ31 samples. The sigmoidal relation between the volume fraction of twins and strain was also shown in [20].

Despite the fact that experimental points, plotted for the coarse- and fine-grained specimens in Fig. 9, seem to follow different types of relation with strain, it was attempted



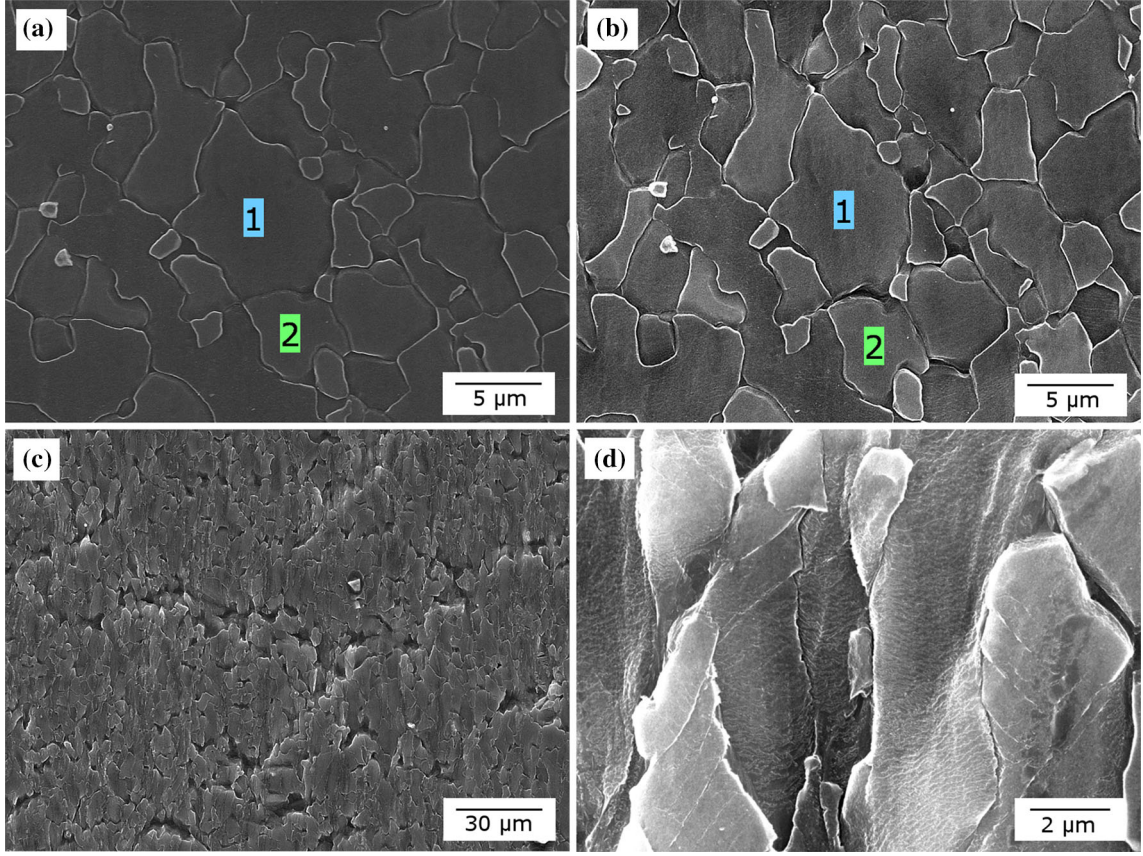


**Fig. 8** Microstructure evolution in the fine-grained sample obtained by I-ECAP and upsetting and tensile tested from initial state (a) to true strain 0.13 (b). Regions near the fracture zone are shown in (c) and (d). Tensile direction is vertical

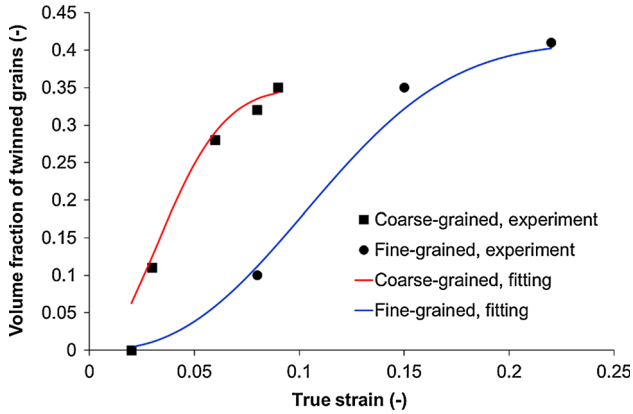


**Fig. 9** Evolution of the volume fraction of twinned grains with strain in the extruded sample (coarse-grained) and in the I-ECAPed sample (fine-grained)

to describe volume fraction of twinned grains,  $V_t$ , by an empirical exponential law [7]:

$$V_t = \left[ 1 - \exp\left(-4\left(\frac{\varepsilon}{\varepsilon_1}\right)^a\right) \right] V_{1t}, \quad (2)$$

where  $\varepsilon$  is macroscopic strain,  $\varepsilon_1$  is macroscopic strain at which the twinning is almost completed (98 %),  $V_{1t}$  is the volume fraction of twinned grains at  $\varepsilon_1$ -obtained from experiment, and  $a$  is the rate exponent. It was assumed in the current study that  $\varepsilon_1$  is the same as fracture strain. The above equation is true for strain larger than 0.025 as the first twins were shown to occur between 0.02 and 0.03 of true strain during in situ observations (Fig. 4). For the lower values of strain,  $V_t$  is equal to zero. As it is shown in Fig. 9, a reasonably good fitting of the Eq. (2) to the experimental results was obtained. The values of coefficients  $a$  and  $\varepsilon_1$  are listed in Table 2.

#### Model fitting to the experimental data

The initial parameters for a model fitting procedure were taken from the literature [8]. It was attempted to keep  $k$ ,  $\eta$ ,  $\xi$  and  $\tau_{0t}$  at the same level as it was in the cited article to allow further comparison of obtained Schmid factors; the parameters are gathered in Table 2. The fraction of twinned grains,  $V_{1t}$ , and the macroscopic strain of twinning completion,  $\varepsilon_1$ , were obtained from experiments so they are

**Table 2** Parameters of Eqs. (4) and (2) for samples after various processing routes obtained in this work and derived from the literature

	$a$	$\varepsilon_1$	$k$ (MPa)	$\eta$	$\xi$	$\tau_{0t}$ (MPa)
Extrusion (parallel to ED)	2	0.09	75	0.2	1.2	45
I-ECAP	2.5	0.22	75	0.2	1.2	45
I-ECAP + upsetting	–	–	75	0.2	–	–
Extrusion (perpendicular to ED) [7]	2.5	0.18	75	0.12	1.4	45

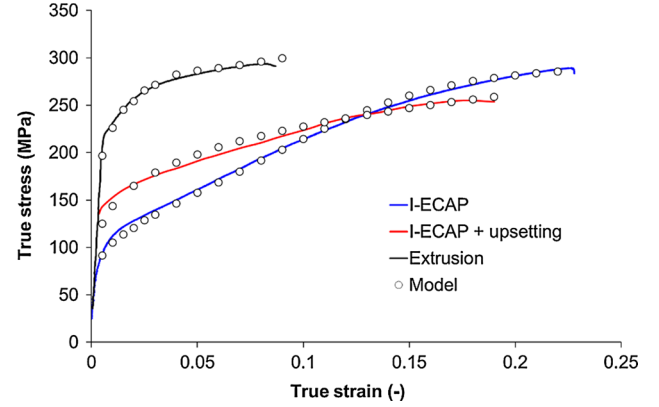
**Table 3** The effective Schmid factors and the volume fractions of twinned grains for various processing routes investigated in this work and derived from the literature

	$m_I$	$m_{II}$	$m_{III}$	$V_{It}$
Extrusion (parallel to ED)	0.48	0.45	0.185	0.35
I-ECAP	0.4	0.215	0.35	0.41
I-ECAP + upsetting	–	–	0.27	0
Extrusion (perpendicular to ED) [7]	0.42	0.22	0.4	0.32
Rolling (parallel to RD) [6]	–	–	0.28	0

not subjected to any changes during fitting of the model. The parameters which are supposed to be varying within the range 0–0.5 for different processing routes are the effective Schmid factors  $m_I$ – $m_{III}$ , the same as in the original model [7]. Their final values obtained in this study and supplemented by the literature data are shown in Table 3.

The fitting procedure was started with selecting optimal values of  $\eta$  and  $m_{III}$  for the sample subjected to I-ECAP followed by upsetting. It was an obvious choice as twinning was not operating in that sample; therefore, the number of sought parameters was smaller than for any other case. It was revealed that  $k$  can be of the same value as in [8] but the hardening exponent,  $\eta$ , must be increased from 0.12 to 0.2 in order to obtain good fitting of the model (Fig. 10). The Schmid factor in the slip-dominated volume (the only volume in this sample) was determined as 0.27.

The obtained hardening exponent ( $\eta = 0.2$ ) was kept constant for the remaining two samples subjected to the fitting procedure. The Schmid factors determined for the I-ECAPed sample were very similar to those obtained during tensile testing perpendicular to ED (Table 3). The results showed that twinning and slip in non-twinned regions occur relatively easily in those samples but microscopic yield stress is increased in zones, where slip operates in already twinned volumes. This mechanism was discussed in [8] and some additional remarks will be given in the discussion section of this article. It should be also noted that the hardening factor,  $\xi$ , of twinned volumes was reduced in this study from 1.4 to 1.2 in order to obtain a better model fitting (Fig. 10).

**Fig. 10** Tensile flow stress curves of the examined samples compared with the modelling results

Finally, the same  $k$ ,  $\eta$  and  $\xi$  as in the case of the I-ECAPed sample were used to model the flow stress curve obtained during tensile testing along ED of the extruded specimen. The best agreement between experimental and numerical data was obtained when  $m_{II}$  was set to 0.45 and  $m_{III}$  was decreased to 0.185. It means that the contribution of slip in the non-twinned volume ( $m_{III}$ ) to the overall stress is higher than in the other samples. It is a reasonable conclusion since deformation dominated by slip (without twinning) occurs up to true strain  $\sim 0.025$  at a high level of macroscopic stress (220–265 MPa), as it was shown through in situ analysis (Figs. 3, 4). Additionally, it was shown that twinning led to decrease in strain hardening rate since stress level due to slip in twinned region was relatively low, which was quantitatively described by the high value of  $m_{II}$ . It suggests that twinning mode in the extruded sample subjected to tension along ED was different from that operating in the I-ECAPed sample.

## Discussion

### Influence of twinning on the strain hardening rate

Mechanical tests showed that strain hardening rate was higher in the I-ECAPed sample than in the I-ECAPed and upset one. The only microstructural feature which was



different for both samples was the occurrence of twinning in the former one. The dominating twinning mode in the I-ECAPed sample is  $\{10\text{--}12\}$  twinning as twin boundaries oriented at  $86^\circ$  were revealed in the EBSD analysis after tensile testing, as shown in Fig. 11. Moreover, the shape of the flow stress curve is similar to the curve obtained in tensile testing conducted perpendicular to ED in [8], where tensile twinning was suspected to be responsible for the increased strain hardening rate. The effective Schmid factor for slip in the twinned volume obtained in this study was smaller than in the other volumes, which shows that slip in those regions is continued with a higher yield stress than before twinning. It can be attributed to the lattice rotation by  $86^\circ$  due to  $\{10\text{--}12\}$  tensile twinning. Stress increase with straining could be also arising from the interactions between dislocation movement and twin boundaries.

The quantitative description, expressed in terms of Schmid factors, showed that the increased strain hardening rate in the I-ECAPed sample due to slip in the twinned regions is similar to that observed in the extruded rod tested perpendicular to ED, as shown in Table 3. Moreover, the sample subjected to upsetting after I-ECAP exhibited almost the same Schmid factor for slip as it was reported before for the rolled plate (Table 3). This similar behaviour can be easily explained by the texture produced in the material by I-ECAP followed by upsetting which is almost

the same as after rolling. It should be noted here that  $k$  and  $\eta$  were greater in the cited article [6]. Nevertheless, the results obtained using the developed model can be relatively easily compared with the literature and conclusions on activation of different deformation mechanisms can be made by analysing the determined effective Schmid factors (Fig. 12).

The flow behaviour of the extruded sample was tested in tension along ED. Twinning in this case was shown to be responsible for decrease in hardening rate after exceeding true strain  $\sim 0.025$ , which was recognised in the in situ test as the onset of twinning. Modelling showed that this behaviour can be explained by increased Schmid factor for slip in the twinned volume. In contrast to the I-ECAPed sample and the extruded sample tested perpendicular to ED [8], twinning was shown to reorient the lattice to the position favourable for slip so the further deformation is continued with a lower stress. Such rotation, resulting in strain localisation within a twin, was already shown in the literature to be caused by  $\{10\text{--}11\}$  contraction and  $\{10\text{--}12\}$ – $\{10\text{--}11\}$  double twinning [2, 4, 5]. Texture measurement of the extruded rod (Fig. 2d) revealed that the c-axes are aligned perpendicular to ED, which means that

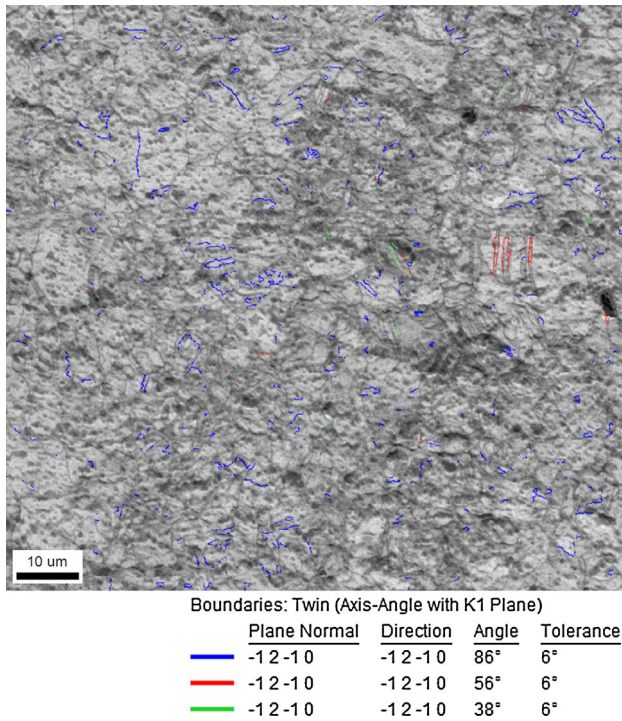


**Fig. 11** EBSD image displaying twin boundaries in the I-ECAPed sample after tensile testing to fracture

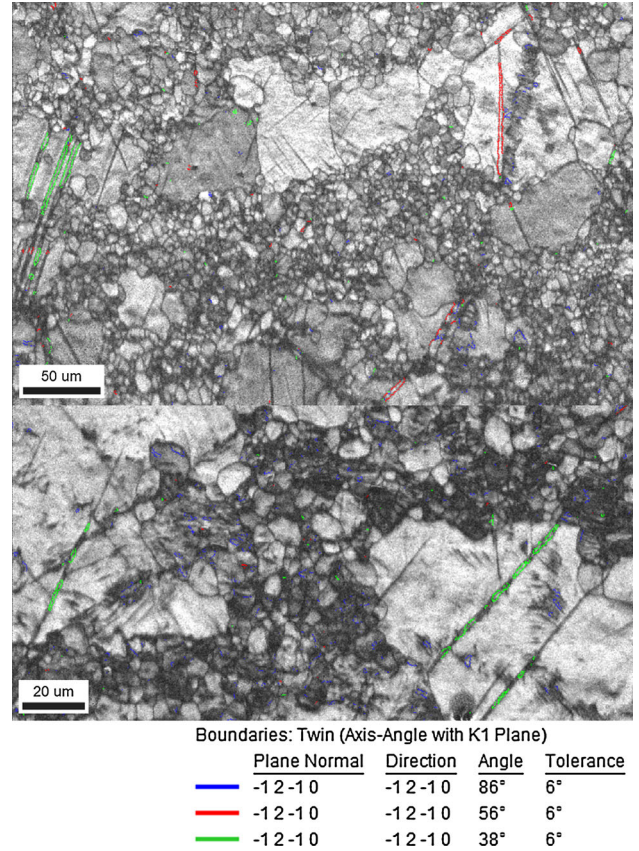


**Fig. 12** EBSD images displaying twin boundaries in the extruded sample after tensile testing to fracture



they are in compression state during tension along ED and this kind of deformation can be satisfied by twinning. This conclusion is also supported by the EBSD observations conducted in this work, which revealed the occurrence of narrow-banded twins oriented at  $56^\circ$  and  $38^\circ$ , recognised as contraction and double twins, respectively. The softening effect of contraction twinning is captured by the model and it is expressed in terms of the high effective Schmid factor for slip in the twinned volume,  $m_{II} = 0.45$ , compared to the hardening effect of tensile twinning expressed as  $m_{II} = 0.215$ .

Finally, some additional remarks on a physical meaning of parameters incorporated in the constitutive model should be made here. The original model [7] was developed to describe influence of tensile twinning on flow behaviour in AZ31 magnesium alloy. In the present work, the attempt was made to capture effects of the different types of twins. As a consequence, contributions from the different twinning modes to macroscopic yield stress are described by only one parameter, the effective Schmid factor. It means that the model reflects the average influence of twinning rather than separate effects of its different types. Therefore, if the microstructure is dominated by tensile twins with a minor part of contraction twins, the Schmid factor for slip in the twinned volume ( $m_{II}$ ) is lower than in the opposite case. However, the low Schmid factor  $m_{II}$  does not indicate that contraction twins are not present and vice versa. Additionally, contributions from slips on the different planes (basal, prismatic,  $\langle c + a \rangle$ ) are described in the current model using only one effective Schmid factor ( $m_{III}$ ).

#### Microstructural effects on fracture mechanisms

Three samples with different processing histories were tested in the current work and each of them exhibited different modes of fracture. The intergranular fracture was shown to be a microstructural feature leading to failure of the I-ECAPed and upset sample. The occurrence of voids can be attributed to stress incompatibilities at grain boundaries arising from different crystallographic orientations of neighbouring grains, which was already predicted in the simulation of microstructure evolution in Mg–Ca magnesium alloy [21]. The failure in the coarse-grained sample examined in this work was shown explicitly to be caused by formation of microcracks within twins. On the other hand, twinning in the I-ECAPed sample was not found to have the same effect since the failure occurred along mesoscopic shear bands, which coincided with the shear plane of I-ECAP.

It was shown in the previous section that twinning has different effects on the flow stress evolution in the extruded rod than in the I-ECAPed sample. Therefore, it could be

concluded that contraction twinning, revealed in the extruded rod, resulted in the earlier fracture of the sample through shear localisation within twins, which led to microcracking. In contrast to the extruded rod, there was no direct relation between twinning and fracture in the I-ECAPed sample as failure along shear bands was revealed.

The influence of yield stress of the twinned volume on local fracture occurrence has been already investigated using FE simulation in our previous work [22]. A twin-like inclusion was introduced to a round particle simulating a grain, which was placed in a matrix. Ideally plastic behaviour of the twin was assumed with the arbitrary yield stresses of 200 and 500 MPa, which are roughly corresponding to the calculated Schmid factors of 0.45 and 0.215, respectively. It was revealed that the zone of maximum tensile stress is located in the corners of the softer twin while the same tensile stress zone was more uniformly distributed within the parent grain and the matrix for the harder twin variant. This simple approach confirmed that fracture is localised within twins with the high effective Schmid factor for slip in the twinned volume, determined in this work as 0.45. The numerical prediction of initiation and propagation of a microcrack within a twin was also displayed in [22].

#### Summary and conclusions

Three types of samples were tested in tension in the present study to investigate the influence of twinning on the strain hardening rate and fracture mode in the AZ31B magnesium alloy. The samples were obtained by (1) direct extrusion (as-supplied), (2) four passes of I-ECAP and (3) four passes of I-ECAP followed by side upsetting. It was shown through in situ and ex situ microstructural characterisations that twinning was not operating in the sample subjected to upsetting, while large twinned regions were observed in the extruded as well as in the I-ECAPed samples.

The flow stress modelling and conducted experiments showed that tensile twinning increases strain hardening rate while the opposite is observed for contraction twinning. The effective Schmid factors for slip in the volumes deformed by tensile and contraction twinning were determined in this work as 0.215 and 0.45, respectively.

Twinning has been also shown to be responsible for an earlier fracture of the extruded sample since microcracking was shown explicitly to be initiated within twins. According to the modelling results, contraction twins are suspected to act as sites for fracture initiation since they result in a shear localisation within the twinned volume.

**Acknowledgements** Financial support from Carpenter Technology Corporation is kindly acknowledged. Part of this research was supported by the Engineering and Physical Sciences Research Council [Grant Number EP/G03477X/1].

**Open Access** This article is distributed under the terms of the Creative Commons Attribution License which permits any use, distribution, and reproduction in any medium, provided the original author(s) and the source are credited.

## References

1. Yoshinaga F, Horiuchi R (1963) Deformation mechanisms in magnesium single crystals compressed in the direction parallel to hexagonal axis. *Trans Jpn Inst Met* 4:1–8
2. Wonsiewicz BC, Backofen WA (1967) Plasticity of magnesium crystals. *Trans Metall Soc AIME* 239:1422–1431
3. Kelley EW, Hosford WF (1968) Deformation characteristics of textured magnesium. *Trans Metall Soc AIME* 242:5–13
4. Al-Samman T, Gottstein G (2008) Room temperature formability of a magnesium AZ31 alloy: examining the role of texture on the deformation mechanisms. *Mater Sci Eng A* 488:406–414
5. Barnett MR (2007) Twinning and the ductility of magnesium alloys. Part II: contraction twins. *Mater Sci Eng A* 464:8–16
6. Marya M, Hector LG, Verma R, Tong W (2006) Microstructural effects of AZ31 magnesium alloy on its tensile deformation and failure behaviors. *Mater Sci Eng A* 418:341–356
7. Barnett MR, Keshavarz Z, Ma X (2006) A semianalytical Sachs model for the flow stress of a magnesium alloy. *Metall Mater Trans A* 37:2283–2293
8. Barnett MR (2007) Twinning and the ductility of magnesium alloys. Part I: tension twins. *Mater Sci Eng A* 464:1–7
9. Yoo MH (1981) Slip, twinning and fracture in hexagonal close-packed metals. *Metall Mater Trans A* 12:409–418
10. Tomé CN, Maudlin PJ, Lebensohn RA, Kaschner GC (2001) Mechanical response of zirconium—I. Derivation of a polycrystal constitutive law and finite element analysis. *Acta Mater* 49:3085–3096
11. Rosochowski A, Olejnik L (2007) FEM simulation of incremental shear. *AIP Conf Proc* 907:653–658
12. Rosochowski A, Olejnik L (2011) Incremental equal channel angular pressing for grain refinement. *Mater Sci Forum* 674:19–28
13. Gzyl M, Rosochowski A, Pesci R, Olejnik L, Yakushina E, Wood P (2014) Mechanical properties and microstructure of AZ31B magnesium alloy processed by I-ECAP. *Metall Mater Trans A* 45:1609–1620
14. Rosochowski A, Olejnik L, Richert M (2008) Double-billet incremental ECAP. *Mater Sci Forum* 584–586:139–144
15. Langdon TG (2007) The principles of grain refinement in equal-channel angular pressing. *Mater Sci Eng A* 462:3–11
16. Gzyl M, Rosochowski A, Yakushina E, Wood P, Olejnik L (2013) Route effects in I-ECAP of AZ31B magnesium alloy. *Key Eng Mater* 554–557:876–884
17. Gzyl M, Rosochowski A, Olejnik L, Reshetov A (2014) The effect of initial grain size on formability of AZ31B magnesium alloy during I-ECAP. *Key Eng Mater* 611–612:573–580
18. Koike J, Ohyama R, Kobayashi T, Suzuki M, Maruyama K (2003) Grain-boundary sliding in AZ31 magnesium alloys at room temperature to 523 K. *Mater Trans* 44:445–451
19. Koike J (2005) Enhanced deformation mechanisms by anisotropic plasticity in polycrystalline Mg alloys at room temperature. *Metall Mater Trans A* 36:1689–1696
20. Jiang L, Jonas JJ, Mishra RK, Luo AA, Sachdev AK, Godet S (2007) Twinning and texture development in two Mg alloys subjected to loading along three different strain paths. *Acta Mater* 55:3899–3910
21. Milenin A, Byrska DJ, Grydin O (2011) The multi-scale physical and numerical modeling of fracture phenomena in the MgCa0.8 alloy. *Comput Struct* 89:1038–1049
22. Gzyl M, Rosochowski A (2013) FE simulation of magnesium alloy microstructure evolution in tension. *AIP Conf Proc* 1567:776–779